ADVANCED INTELLIGENT SYSTEMS
Open Access
www.advintellsyst.com

# A Magnetorheological Elastomer-Based Proportional Valve for Soft Pneumatic Actuators

*Sihan Wang,* Liang He, Alessandro Albini, Peizhi Zhang, and Perla Maiolino*

**The interest in soft pneumatic actuators has been growing rapidly in robotics, owing to the contact adaptability with the material softness. However, these actuators are mostly controlled by rigid electronic pneumatic valves, which can hardly be integrated into the robot itself, limiting its mobility and adaptability. Recent advances in soft or electronics-free valve designs provide the potential to achieve an integrated soft robotic system with reduced weight and rigidity. Nevertheless, the challenge in valve response remains open. To enable dynamic control of a soft pneumatic actuator (SPA), a fast-response proportional valve is needed. Herein, the potential of Ecoflex-based magnetorheological elastomer (MRE) membrane to create a proportional valve that can be used in the control of a soft robot made from the same silicone material is explored. Experimental characterization shows that the proposed MRE valve (30 mm × 30 mm × 15 mm, 30 grams) can hold pressure up to 41.3 kPa and regulate the airflow in an analog manner. The valve is used to perform closed-loop proportional–integral–differential (PID) control with 50 Hz on a SPA and is able to control the pressure within the actuator chamber with a root-mean-square error of 0.05 kPa.**

## 1. Introduction

Soft robots driven by soft pneumatic actuators (SPAs) are known for their low cost, high adaptability to unknown environments, and safe human–robot interaction.[1] As an emerging area, researchers have developed various SPAs with different materials, structure designs, actuation modes, pressure ranges, and fabrication procedures.[2] A basic design principle has been carried out in most of the SPAs: the actuation is achieved by mediating the interaction between pressurized air and soft elastomeric materials. The dexterity, mobility, and efficiency of a SPA ultimately depend on the control of pressure. Previously, this pressure control was achieved mainly by conventional pneumatic systems, including solenoid valves, proportional regulators, displacement pumps, syringe drivers, and electronic controllers.[3,4] These bulky and nonintegrable devices limit the performance of pneumatic-driven soft robots, carrying challenges for the robot to be miniaturized, untethered, and agile.

These existing limitations motivate researchers to develop different lightweight and integrable control devices for regulating pressure in SPAs. One category is the pneumatically driven soft valves, which directly receive pneumatic signals and correspondingly regulate the pressure in the pneumatic actuators.[5] Various fabrication techniques have been used including silicone casting[5] and 3D printing.[6] These devices can be used as the pneumatic correspondent of various electronic components including transistors, diodes,[7] oscillators, logic gates,[8] digital–analog converters (DACs),[9] and digital memories.[10] Pneumatically driven soft valves bring simplicity to the system as the conversion of sensory information into electrical signals is no longer required. The soft structure also means these valves can be integrated into the robots themselves without sacrificing the overall compliance of the robots. However, these devices come with a relatively long response time (ranging from 0.5 to 1.5 s), which limits their application in control.

Electrostatic effect[11] and dielectric effect[12] have also been investigated in valve designs for controlling SPAs, introducing faster response time, but require a high operation voltage. The requirement of voltage amplifiers limits their application in soft robots, especially when the robot is demanded to be untethered and miniaturized.

The devices listed above work in a digital ON/OFF manner. However, recent applications of soft robots require not only binary ON/OFF control, but also proportional control on their pressure or flowrate. The ability to continuously alter the pressure or flowrate of soft robots in an analog manner provides advantages in various applications. In human–robot interaction[13] and adaptive grasping,[14] the proportional pressure control is essential for controlling the interactive force between the actuator and its environment. For soft pneumatic manipulators,[15] the proportional pressure control is the key for trajectory following. In soft-matter computing,[16]

S. Wang, L. He, A. Albini, P. Maiolino
Department of Engineering Science
University of Oxford
Oxford OX1 3PJ, UK
E-mail: sihan.wang@eng.ox.ac.uk

P. Zhang
Research Innovation Center
Waseda University
Shinjuku-ku, Tokyo 162-0041, Japan

The ORCID identification number(s) for the author(s) of this article can be found under https://doi.org/10.1002/aisy.202200238.



**DOI: 10.1002/aisy.202200238**

continuously altering the flowrate enables us to fine tune the frequency of an oscillating pneumatic signal.

The most widely used devices for continuously altering the pressure are syringe drivers[3] and industrial proportional valves.[17] These highly accurate and robust approaches are usually bulky and nonintegrable for soft robots. Moreover, the syringe drivers cannot deliver a large flowrate and therefore are slow in response time.

Recent research has attempted the proportional pressure control of soft robots using electropermanent magnets (EPM).[18] By adjusting the magnetic field strength, the device can continuously alter its fluidic resistance and therefore modulate the pressure. However, this device is only capable of controlling soft robots driven by magnetorheological fluid, which narrows down its application since many soft robots are driven by compressed air.

Another solution for proportional pressure or flowrate control on a fluid-driven actuator is using thermally-driven hydrogels.[19] The physical properties of such devices (reflected in the fluidic resistance) are controlled by temperature to achieve adjustment of the flowrate and pressure of fluidic-driven soft actuators. However, a long response time (over 20 min) is usually required, which brings limitations for most soft robotic applications.

Recent developments in magnetorheological elastomers (MRE) show that this soft magnetoactive rubber-like material has the advantages of continuously adjustable mechanical characteristics[20] and fast response time[21,22] under magnetic actuation. The interaction between the MRE and the magnetic field has been exploited in designing various actuators. Microfluidic pumps and mixers based on MRE[23] have been used in microfluidic platforms. Soft actuators[24] and grippers[25–27] have been developed, which make use of the force exerted by MRE when placed within a magnetic field. In addition, MREs can be used as highly deformable robot skin for proprioception in SPAs.[28] An MRE valve[29] has also been designed based on its deformation under a magnetic field, although the valve is based on a highly bulky and rigid mechanism, which limits its application in soft robots. Recently, MRE has been applied in the soft robotics field, thanks to its compliant nature and its ability to be integrated into silicone-based soft robots.[24,26] The softness of the material and its capability to bond to silicone rubber indicate the potential of developing an MRE-based valve to be integrated with SPAs for fast and precise fluidic control.

Thus, this article presents the design of a proportional valve for controlling SPAs based on an MRE membrane. The valve makes use of an electrical coil embedded in silicone to generate a magnetic field and therefore control the MRE membrane movement. The valve behavior was characterized by two aspects: 1) the variation in flowrate of the valve under different electric currents and 2) the maximum pressure held by the valve without leaking under different electric currents. The valve behaviors with different MRE membrane thicknesses and air channel widths were investigated. To demonstrate the applications of the MRE valve designed, the valve was used to perform closed-loop flowrate and pressure control on SPAs. It was observed that the valve can control the pressure within the actuator chamber with a root-mean-square error (RMSE) of 0.05 kPa.

## 2. Results

### 2.1. MRE Valve Design

#### 2.1.1. Valve Structure and Working Principle

The MRE valve consists of an electromagnet and an MRE membrane to create the valve gate. **Figure 1**A shows the cross-sectional view of the proposed valve. The electromagnet is sealed in silicone to ensure maximum compliance. The gate of the valve is designed by encapsulating a pressurized cavity between the MRE membrane and the electromagnet. The detailed dimensions of the valve can be found in Supporting Information S1. The proposed valve works in a "normally open" manner, as shown in Figure 1B. When no current goes through the coil, no force is exerted by the MRE, so air travels freely through the air channel. When an electric current is engaged in the coil, a magnetic field will be generated. The MRE is then magnetized and a force is exerted toward the concentration of the magnetic flux. This attraction force deforms the MRE and correspondingly restricts the gate of the valve. This "restriction" effect gradually increases as the electric current increases and eventually shuts down the airflow completely. A video presenting the working principle of the MRE valves can be found in Video SV2, Supporting Information.

#### 2.1.2. Fabrication

Multistage silicone casting is used to fabricate the MRE valve presented in this work. The detailed fabrication procedure is presented in Figure 1C. The first stage of casting aims to seal an electromagnet into a silicone housing. This is achieved by placing the electromagnet into a cylindrical mold filled with uncured silicone. The second stage of casting aims to build an MRE layer on top of the electromagnet while leaving an air channel inside. This is achieved by pouring the uncured MRE on top of the electromagnet. A mylar strip is placed in the middle during MRE's curing and pulled out afterward, therefore leaving a thin air channel as the gate of the valve. A video describing the whole fabrication process can be found in Video SV1, Supporting Information, while the technical details involved can be found in Section 4.

### 2.2. Experiment Characterization

#### 2.2.1. Optimal Carbonyl Iron Powder Content Level

It was shown in literature[30] that the saturation magnetization improves by increasing the content of the carbonyl iron powder (CIP). Creating MRE with high CIP content is beneficial to the valve design as it decreases the electric current required to regulate the airflow. However, higher CIP content in MRE results in significantly reduced flexibility and difficulties in polymerization. The bonding between the MRE membrane and the silicone base of the valve can also be an issue. To investigate the optimal CIP content level for fabricating the MRE valves, a set of samples as shown in **Figure 2**A were tested. These samples were made by bonding an MRE membrane (2 mm thickness) to a silicone membrane (2 mm thickness) while leaving an air channel in their middle. The detailed schematics used for the experiments

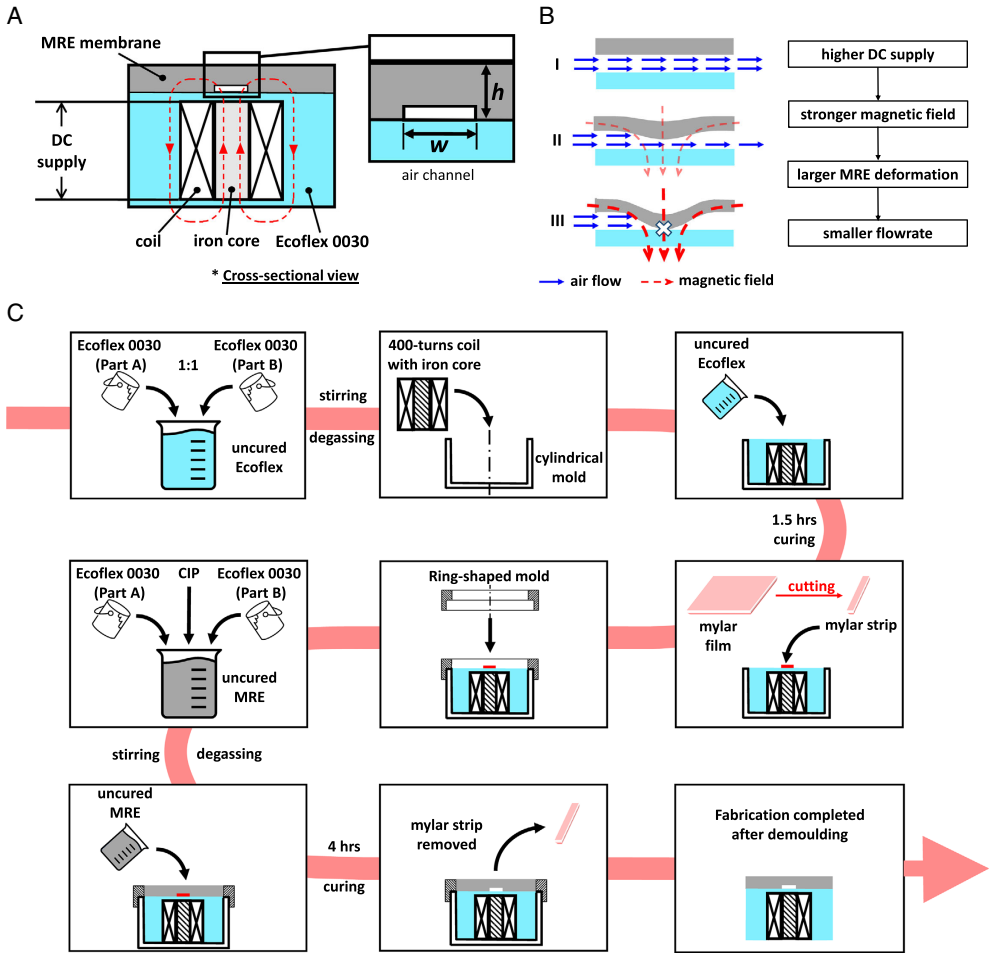


**Figure 1.** A) The structure of the MRE valve. B) The concept and working principle of the valve. The detailed views of the air channel explain how the deformation of the MRE valve affects the airflow through the channel. An increase in electric current results in a stronger magnetic field. This brings more deformation to the MRE membrane and therefore decreases the flowrate. C) The fabrication process of the MRE valve.

are shown in Figure 2B. The pressure within the air channel of the samples was gradually increased until the sample fails and the pressure was monitored during the whole process. The pressure at failure was then recorded. For each CIP content level, three identical samples were made and tested. The mean and standard deviation of the pressure at failure for different CIP levels are presented in Figure 2C. Two different failure modes were observed. For samples with a CIP level of no more than 80 wt%, the MRE membrane undergoes a burst in its center under high pressure and leaves a crack. The pressure at failure here is consistently higher than 150 kPa. For CIP levels higher than 80 wt%, the MRE layer delaminates from the silicone layer, indicating that the bonding between the two layers is the dominant weakness. The pressure at failure here drops significantly below 50 kPa. The standard deviation also increases, indicating a lack of consistency for samples with too high CIP levels. This inconsistency is most likely brought in during the fabrication process, as the higher CIP level significantly increases the viscosity of the uncured MRE and therefore makes it difficult to be cast into an even-thickness MRE membrane. Based on the results presented in Figure 2C, the CIP content level chosen for fabricating the MRE valves is 80 wt%, as it is the highest CIP level achieved without sacrificing too much strength.

To further investigate the structure of the 80 wt% MRE, a scanning electron microscope (SEM) was used. Both the surface and the middle of the sample were examined by the SEM, aiming to investigate the structure consistency throughout the sample. Note that the sample was cut with a knife to observe the interior. The obtained SEM images are shown in Figure 2D,E. As shown in Figure 2D, no significant difference were found between the MRE structure at its surface and middle, indicating a good structural consistency throughout the sample. Despite the relatively large weight ratio, the iron particles are uniformly distributed within the silicone in both images. This homogeneous particle distribution is of benefit as it ensures the repeatability and consistency of the MRE membrane behavior. Figure 2E represents a 3000× magnified SEM image of the interior of the sample. This SEM image with larger amplification ratio clearly shows that the CIP participles are firmly embedded into its silicone matrix, therefore bringing sufficient structural stability.

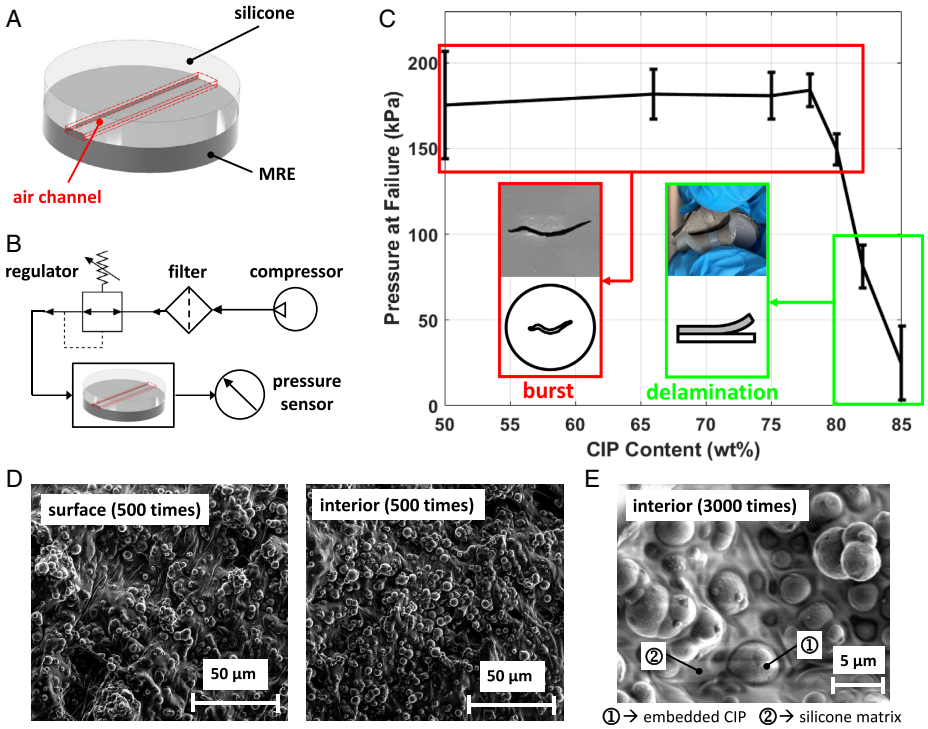


**Figure 2.** Maximum allowable pressure held by the MRE membrane against different CIP levels. A) The structure of the samples used in this experiment. B) The experiment schematics used in this experiment. C) The pressure at failure of the MRE membrane with different CIP content level. The errorbar indicates the standard deviation among three samples. D) The 500× magnified SEM images of the 80 wt% MRE sample at its surface and interior. E) The 3000× magnified SEM image of the 80 wt% MRE sample at its interior.

### 2.2.2. Membrane Geometry

Finiteelement simulation (implemented in Comsol Multiphysics 5.6, detailed setup in Section 4) shows that the maximum magnetic flux density occurs at the annular region at the edge of the iron core. The magnetic field generated by the coil at the plane of the air channel is shown in **Figure 3**A. To investigate the impact of MRE membrane geometry on valve performance, four different MRE membrane geometries (shown in Figure 3B) were fabricated and tested based on the simulated magnetic field. All four geometries cover the annular region with the strongest magnetic field. The simulated magnetic fields with different MRE geometries are shown in Figure 3C. The FE simulation shows that the "Full" and "Parallel line" provides the strongest magnetic field strength within the air channel. The larger magnetic flux density indicates that the MRE membrane can more effectively regulate the airflow given the same amount of electric current. To validate the simulation, four samples with different MRE geometries were fabricated and tested.

Experimental validation is performed with a constant input pressure of 20 kPa, while the detailed schematics are shown in Figure 3D. The experimental results are shown in Figure 3E. The valve with "Full" geometry shows the best performance, which successfully shuts down the 20 kPa incoming flow with a minimum electric current of 2.25 A. The valve with "center" geometry is able to shut down the 20 kPa incoming flow only when the electric current reaches 3 A. Based on these results, the MRE geometry chosen for fabricating the MRE valves is the "Full" geometry, due to its optimal performance and ease of fabrication.

### 2.2.3. Effect of the MRE Thickness on Valve Behavior

The behavior of the MRE valves is mainly described by the following two aspects: 1) the threshold pressure and 2) the flowrate under different current supplies (flowrate–current profile). Threshold pressure is defined as the maximum pressure the valve can withstand without leaking when the electrical current is engaged in the coil. This value is of interest as it ensures the valve can deliver enough pressure to drive the pneumatic soft actuators efficiently. The flowrate–current profile confirms the valve can be operated in an analog manner with repeatability. With increasing current, the airflow decreases monotonically due to the increase of the magnetic force and the reduction of the opening width of the valve channel. This variable pneumatic resistance can be used to control the SPAs similar to an industrial proportional valve.

To investigate the effect on valve behavior brought by the different MRE membrane thicknesses, samples with membrane thicknesses ranging from 1 to 3 mm with a step size of 0.5 mm were tested. The flowrate and threshold pressure characterization results are presented in **Figure 4**A,B, respectively.

Figure 4A indicates that the increase in MRE thickness significantly enhances the regulation of the airflow. As the MRE

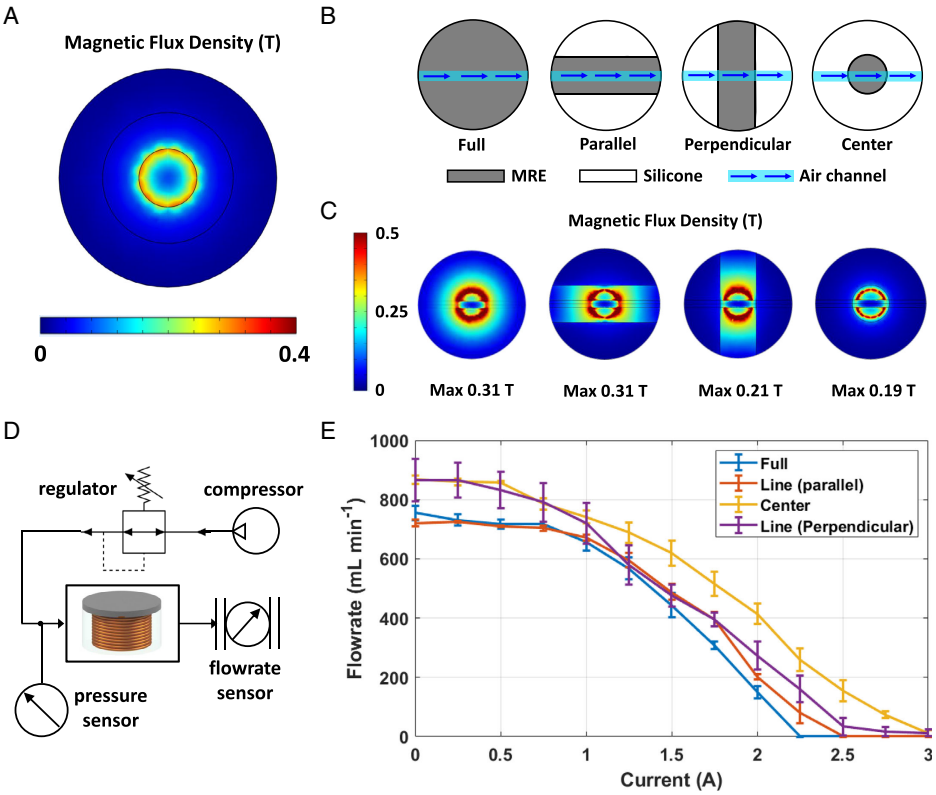


**Figure 3.** A) The simulated magnetic flux density generated by the coil itself at the top surface of the coil. B) The four different MRE geometries investigated. C) The simulated magnetic flux density at the plane of the air channel, with different MRE membrane geometries. D) The schematics of the physical experiments and E) the flowrate–current curve of the MRE valves with different MRE membrane geometries. The errorbar indicates the standard deviation among three different trials.

thickness increases from 1 to 3 mm, the electric current required to fully shut down the flow decreases from over 3 to 1.75 A. This is because the increase in MRE membrane thickness increases the exerted attractive force due to more magnetization, meaning that a weaker magnetic flux density is required to shut down the flow. However, one should also note that the flowrate of the valve without electric current ("fully open" state) is decreased by a thicker MRE membrane, even if the air channel width is kept constant. As the MRE thickness increases from 1 to 3 mm, the flowrate without electric current decreases by 33.1%. This is because the thicker MRE performs less deformation when air passes beneath it.

### 2.2.4. Effect of the Air Channel Width on Valve Behavior

As shown in Figure 4A, the increase in MRE membrane thickness not only decreases the current required to regulate the airflow, but also decreases the volume flowrate when the valve is in its fully "open" stage (with no electric current going through). This lack of flowrate is undesirable as it increases the response time of the soft robots with large internal volumes. One possible way to easily compensate for the flowrate reduction is by increasing the width of the air channel. This can be easily achieved by increasing the width of the mylar strip used during the fabrication. Three samples with different air channel widths (1, 2, and 3 mm) were fabricated here and tested. The obtained characterization results are shown in Figure 4C,D.

As shown in Figure 4C, the increase in air channel width significantly scales up the volume flowrate. The valve with a 3 mm channel width brings an additional 406% flowrate at "fully open" state, compared with the one with a 1 mm channel width. Meanwhile, the electric current required to fully shut down the airflow does not see a significant change as the channel width increases. (see Figure 4D).

### 2.2.5. Temperature Response

The heat generated during the operation of the valve inevitably increases its temperature, therefore potentially changing the performance and characteristics of the valve. This experiment aims to investigate the performance of the valve during long-term continuous operation, including the temperature and the flowrate through the valve. An MRE valve sample with 3 mm channel width and 2 mm MRE thickness was used here. A constant electric current was applied to the coil. The temperature of the valve was kept monitored throughout the process by a temperature sensor placed in the middle of the bottom surface of the valve. The input pressure of the valve was kept at 20 kPa. The temperature and flowrate curves under three different levels of electric current (1, 1.75, and 2.5 A) were tested and are presented in

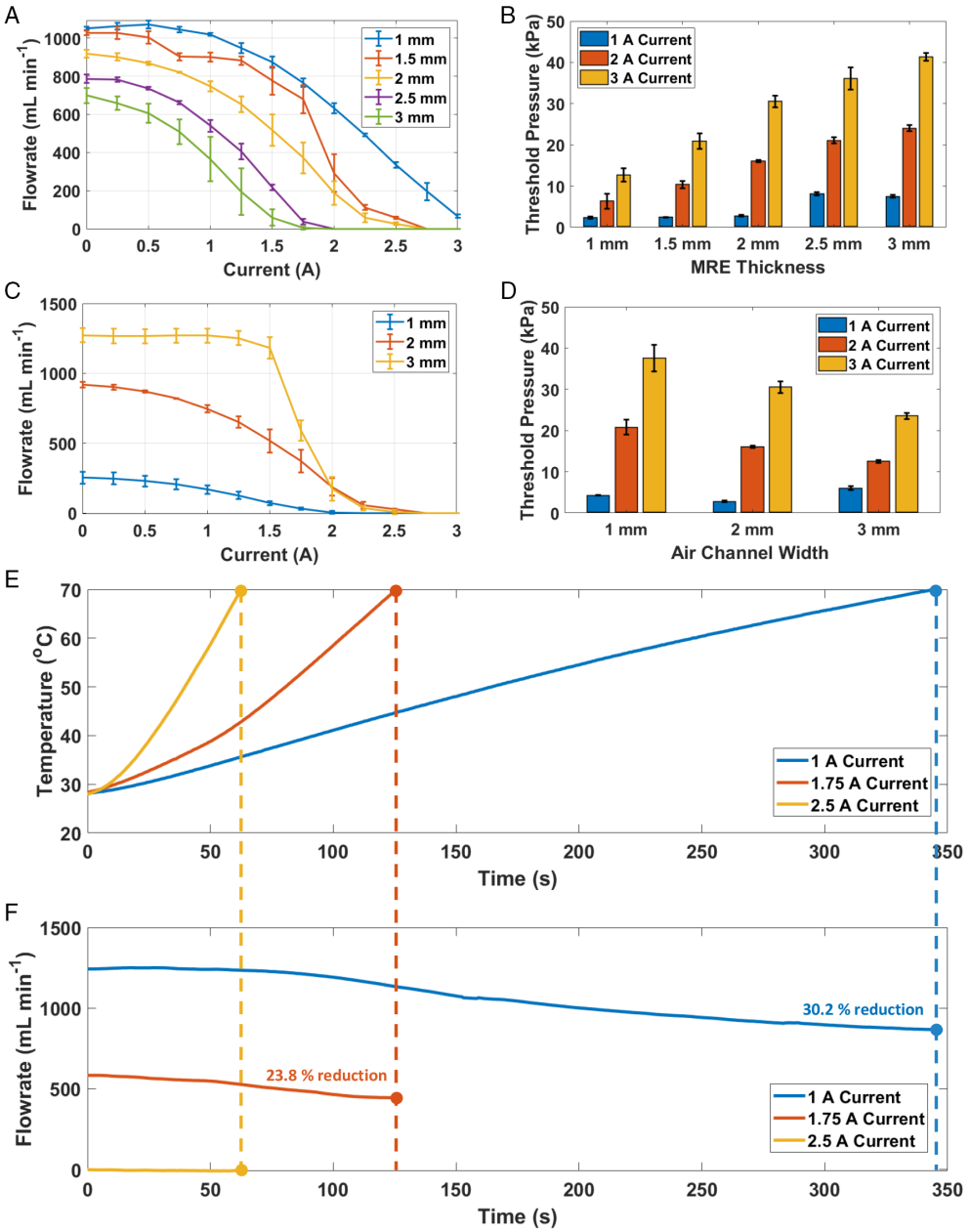


**Figure 4.** Characterization of the MRE valve behavior with different design dimensions. A) The flowrate–current curve of the MRE valves with different MRE thicknesses. B) The threshold pressure of the MRE valves with different MRE thicknesses. C) The flowrate–current curve of the MRE valves with different channel widths. D) The threshold pressure of the MRE valves with different air channel widths. E) The temperature profile of the MRE valves under different amount of electric current, while F) presents how the flowrate of the valve changes during the temperature increase.

Figure 4E,F. These electric current values were selected as they cover the range within which the pneumatic resistance of the valve changes most rapidly, according to Figure 4C. The test was stopped when the surface temperature reaches 70 °C for safety. Sufficient time (1 h) was placed between each trial to ensure that the valve returns to the ambient temperature.

It can be observed that it takes 62, 130, and 348 s for the MRE valve to reach 70 °C with a continuous electric current of 1, 1.75, and 2.5 A, respectively. This temperature rise does not change the basic working principle or the overall behavior of the valve qualitatively. The increase in current still brings a decrease in flowrate and eventually shuts down the airflow. However, the quantitative behavior of the valve does have a certain sensitivity to the temperature. The flowrate through the valve channel sees a 30.2% and 23.8% reduction over the entire heating process with 1 and 1.75 A electric current, indicating a small increase in the pneumatic resistance due to the temperature change. This thermal drift is most likely caused by the thermal deformation of the

MRE membrane and the silicone. This observed sensitivity to the temperature may affect the control accuracy when the valve is used in an open-loop control scheme, as the valve behavior will slightly differ from the preobtained characterization results. However, this thermal drift can be compensated by a sensory feedback loop with a simple proportional–integral–differential (PID) controller (see Section 2.3), as the basic working principle of the valve remains valid. When 2.5 A current is applied, the valve is able to shut down the airflow completely without leaking throughout the entire heating process.

#### 2.2.6. Durability Test

Cycling tests were performed to investigate the durability of the MRE valve.The tests were preformed by repeatedly activating the MRE valve with 2 mm channel width and 2 mm membrane thickness for 5000 times. For each cycle, an electric current of 2.5 A was applied to the valve for 0.5 s, followed by a resting time of 1.5 s. For safety reasons, the cycling tests were paused every time when the valve temperature exceeded 70 °C and resumed after cooling. The valve behavior (flowrate–current profile and threshold pressure) was tested after every 2500 cycles. Note that the valve was cooled down to room temperature before these tests to isolate the thermal drift from the observations. The measured valve behaviors after 2500 and 5000 cycles are presented in **Figure 5**.

It was observed that the valve does not undergo any significant change in its properties and behaviors after the 5000 cycles. The flowrate–current curve keeps its trend after 5000 cycles and only deviates from the initial values by a RMSE of 55.3 mL min$^{-1}$. The 5000 repeating cycles increase the threshold pressure of the MRE valve by a factor of 11.8%, 24.0%, and 5.9% with a 1, 2, and 3 A electric current, respectively. This minor increase in the threshold pressure can be caused by the fact that the iron participles were slightly reoriented or relocated in the silicone matrix during the cycling tests.

### 2.3. Applications in Controlling Soft Robots

Flowrate and pressure are the two most significant factors to be considered when controlling soft pneumatic robots. To drive these robots accurately, one should be able to continuously regulate these two parameters to the desired values. Therefore, to validate the applications of these MRE valves in controlling soft pneumatic robots, the closed-loop control performance of these valves in both flowrate and pressure regulation was tested. PID controllers were implemented in real time on a microcontroller. The detailed setup, tuning and the PID parameters can be found in Section 4 and Supporting Information. The step responses of the controlled flowrate and pressure were recorded.

#### 2.3.1. Closed-Loop Flowrate Control

For closed-loop flowrate control, the experimental schematic is shown in **Figure 6**A. Constant pressure was supplied to the inlet of the MRE valve, while the MRE valve outlet was connected to the atmosphere via a flowrate sensor. The MRE valve here behaved like a pneumatic resistor whose resistance value can be continuously altered. The reading of the flowrate sensor $q$ was then compared with a reference value $q^*$, which is a step signal in our test. The error between the reference and the actual value was sent into a PID controller. The reference value was also sent into a forward model obtained in Figure 4, which gave the expected amount of electric current required by the valve. The final control signal combined the output of the PID controller and the model. The obtained control signal was then fed into a signal amplifier to control the electric current through the MRE valve. The electric equivalent of the pneumatic circuit used here is presented in Figure 6B. Figure 6C presents the step response of the controlled flowrate under three different control schemes tested. "PID only" means only a PID controller is used in the loop. In this case, the response time at the rising edge is around 0.5 s while the response time at the falling edge is around 0.8 s. No significant steady-state error is observed, and the RMSE during the steady state is 14.37 mL min$^{-1}$. "Model only" means the PID feedback loop is disabled and the valve is controlled in an open-loop manner with only the forward model obtained from Figure 4. A significant error of more than 50 mL min$^{-1}$ is observed, caused by the difference between the actual valve behavior and the preobtained model. The response time at the rising edge is longer than 2 s due to the viscoelasticity of the MRE membrane. However, the response time at the falling edge reduces to 0.15 s, thanks to the feed-forward model. "PID + Model" means the feedforward model is combined with a PID controller to eliminate the model inaccuracy and thermal drift. This scheme shows the best performance among all three schemes. The response times are 0.4 and 0.1 s at the rising and

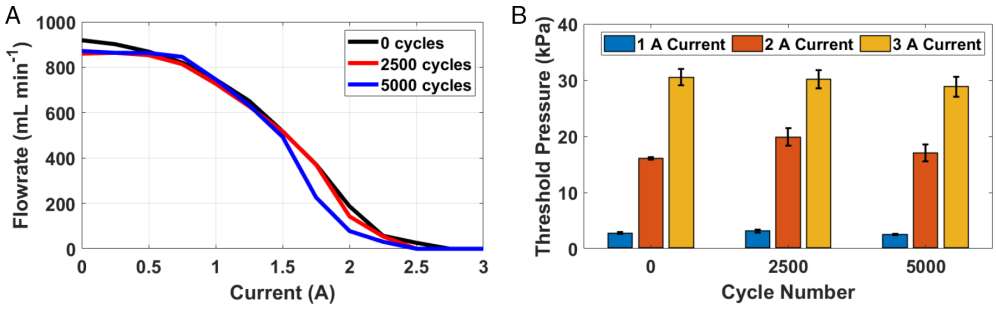


**Figure 5.** Durability performance of the MRE valve under cycling tests. A) The flowrate–current curve of the MRE valves after 0, 2500, and 5000 cycles. B) The threshold pressure of the MRE valves after 0, 2500, and 5000 cycles.

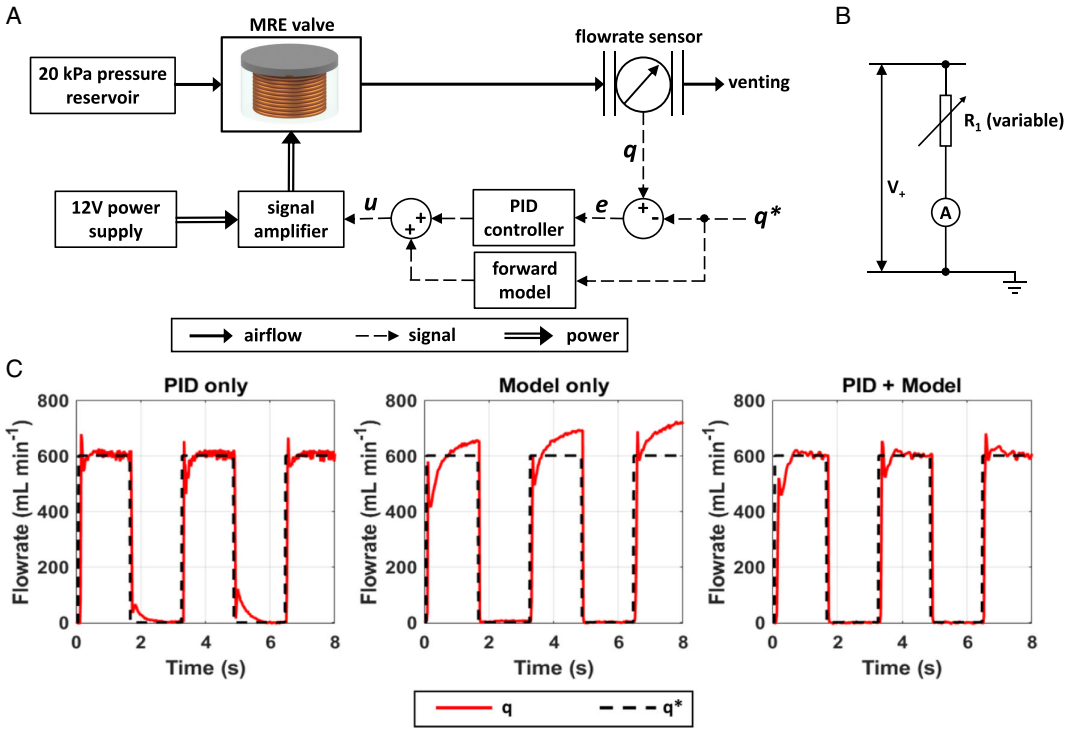


**Figure 6.** Flowrate control achieved by the MRE valves. A) The schematics of the pneumatic and electric circuit used to achieve a closed-loop feedback control on flowrate with the MRE valve. B) An electronic equivalent of the pneumatic circuit used here. C) The step response of the controlled flowrate under different control schemes.

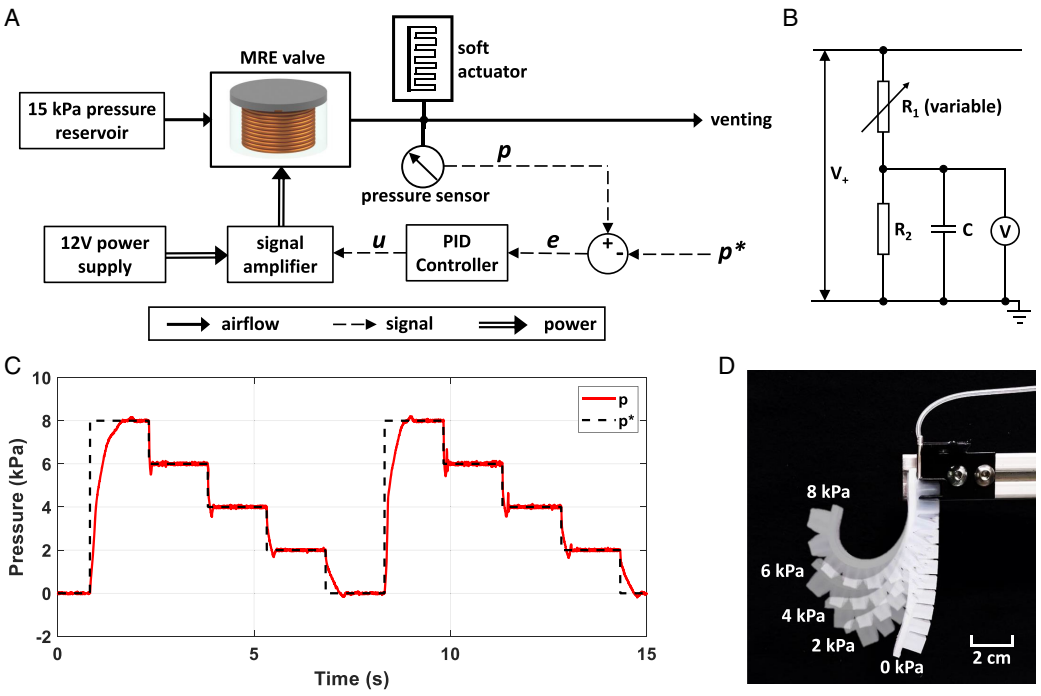


**Figure 7.** Pressure control achieved by the MRE valves. A) The schematics of the pneumatic and electric circuit used to control the pressure within a SPA. B) The electronic equivalent of the pneumatic circuit used for pressure control. C) The step response of the pressure within the SPA controlled by the MRE valve. D) The different amount of bending of the actuator under different desired pressure values.

falling edge respectively. No significant steady-state-error are observed and the RMSE during the steady state is 8.77 mL min$^{-1}$.

#### 2.3.2. Closed-Loop Pressure Control

For closed-loop pressure control, the schematics are shown in **Figure 7**A. The pressure reservoir was set at 15 kPa. The soft actuator (PneuNet, a silicone-casted bending actuator)[31] was placed between the MRE valve and the venting path. When no electric current passes through the MRE valve, it is fully opened. This means the SPA had much lower pneumatic resistance at its upstream than its downstream, therefore bringing a large pressure within the actuator chamber. When a large electric current passed through the valve, the valve was fully closed. In this case, the air inside the chamber would soon escape to the atmosphere and the SPA would return to its natural shape. The pressure reading $p$ in the actuator chamber was then compared with a reference value $p^*$. The error between the actual and reference pressure was then fed into a PID controller (see details in Supporting Information S3), whose output was fed into a signal amplifier to control the electric current in the MRE valve. The electric equivalent of the pneumatic circuit used here is presented in Figure 7B. The MRE valve is equivalent to the variable resistor $R_1$, the natural pneumatic resistance of the venting path is equivalent to the constant resistor $R_2$, and the pneumatic actuator can be seen as a capacitor $C$. Figure 7C presents the step response of the controlled pressure within the soft actuator. The slowest response (0.7 s) occurs when the reference signal goes from 0 to 8 kPa. This is limited by the fluid-dynamic nature of the system, as it takes time for the air to pressurize the large actuator chamber through a relatively narrow valve channel. The RMSE of the controlled pressure at each steady state is 0.05 kPa. Figure 7D presents the postures of the SPA at each steady state. A video of the pneumatic actuator being controlled can be found in Video SV3, Supporting Information.

## 3. Discussion and Conclusions

This paper article a proportional valve which is based on the activation of an MRE membrane. Inspired by the continuous deformation of MRE under a magnetic field, this design utilizes silicone casting to produce an air channel within MRE whose pneumatic resistance can be continuously altered by the magnetic field generated by a coil. Apart from the analog activation manner, this design also ensures a fast response time, operating at a time scale of tens of milliseconds, much shorter than the mechanical response time of most SPAs. Multiple advantages of this MRE valve can be observed when compared with those existing proportional valves used in industries. First, this MRE valve can be integrated into silicone-based soft robots as it is made with compliant MRE and silicone materials. The total cost of the valve is well below $5, which is much lower than its industrial counterparts. Moreover, the valve comes with a simple structure with no moving parts. This brings the valve better mechanical robustness, ease of manufacture, and compatibility with both pneumatic and hydraulic systems. Finally the MRE valve comes with higher accuracy in the lower-pressure region (below 40 kPa), which makes it highly suitable for soft robotic applications.

The experiment characterization proves that the valve can hold pressure up to 41.3 kPa. The valve works in an analog manner, whose pneumatic resistance can be continuously changed by adjusting the electric current through it from 0 to 3 A. Closed-loop flowrate regulation and pressure control with a 50 Hz control frequency were implemented to demonstrate the compatibility and responsiveness of the valve for controlling soft pneumatic robots.

One major limitation existing in the current design is the temperature rise during operation caused by the Joule heating effect. Though this temperature rise does not affect the basic working principle or the overall valve behavior qualitatively, the pneumatic resistance of the valve does exhibit a thermal drift. This may become problematic when the valve is used for open-loop control with no sensory feedback available. This limitation could be addressed in future work by replacing the electric coil with an EPM, applying embedded temperature compensation or introducing a heat dissipation system. In future studies, the size miniaturization and the possibility to pack multiple channels and valves in a circuit will be investigated.

## 4. Experimental Section

*Fabrication of MRE Valve*: The fabrication procedure can be found in Figure 1C. Firstly, equal amount of Part A and Part B of the silicone elastomer (Ecoflex 00-30, Smooth-On, USA) were mixed. Ecoflex 00-30 was a type of platinum-catalyzed silicone with a shore hardness of 00-30. The mixed elastomer was well-stirred and then placed in a vacuum chamber (3CFM/7.6 L, VEVOR, UK) until the formation of new bubbles stops. Meanwhile, a 400-turn coil with an iron core (EK1909U, Gikfun, China) was placed in the center of a 3D-printed cylindrical mold (printed by Creality Ender-5 with 1.75 mm PLA). The mixed and degassed silicone was then poured into the mold until reaching the mold brim. The brim was designed to be slightly higher than the coil, ensuring that the coil can be fully enclosed in silicone. After curing for 1.5 h, the silicone was mostly cured and was strong enough to perform the following fabrication procedures. A sheet of Mylar film (0.075 mm, RS PRO, UK) was cut into strips of 2 mm width. The strip was then placed at the top middle of the silicone cylinder, followed by a ring-shaped mold (printed by Creality Ender-5 with 1.75 mm PLA) attached to the top of the previous cylindrical mold. The uncured MRE was fabricated by combining 5 μm Carbonyl Iron Powder (Sigma-Aldrich, USA) with Ecoflex 00-30. The MRE was well-stirred and degassed in a vacuum chamber until no bubble turns out. After fully being mixed and debubbled, the uncured MRE was then poured into the ring-shaped mold until it reaches the mold brim. After four hours of curing, the poured-in MRE layer bonded firmly with the silicone beneath. The mylar strip was then pulled out gently so that an air channel was formed. Lastly, The MRE valve was removed from the mold.

*SEM Setup*: Platinum sputtering was performed in advance with a sputtering device (MSP-1S, Nissin EM Ltd.) to reduce sample charging and enhance secondary electron emission. The SEM used here is JSM-6510LA, manufactured by JEOL Ltd. The observation was performed at an acceleration voltage of 3 kV and a working distance of 10 mm.

*Magnetic Field Simulation*: The simulation was constructed in COMSOL Multiphysics 5.6, while the specific settings are as followed:

*Magnetic Field Simulation: Geometry Construction*: MRE valves were constructed in COMSOL using the "Geometry" function. Same as the MRE valve in the physical world, it also contained a core (cyl1), a coil (cyl2), a silicone housing (cyl3), and an MRE membrane with a flow pass (cyl4) in the simulation. Additionally, a block was built to cover the entire MRE valve as the surrounding environment (blk1).

*Magnetic Field Simulation: Material Selection*: The materials of cyl1, cyl2, cyl3, cyl4, and blk1 were set to soft iron, copper, silicone, soft iron, and air, respectively. These are the preset materials in the COMSOL library. The relative permeability was 5000 for cy1 (i.e., core), 1 for cy2 (i.e., coil), 10 for cy3 (i.e., silicone housing), 10 for cy4 (i.e., MRE membrane), and 1 for blk1 (i.e., air). Here, we set the relative permeability of the MRE membrane to 10, based on related research on MRE.[32]

*Magnetic Field Simulation: Physics Study*: "Magnetic Field" was selected as the physics study by using the "Add Physics" function. In the "Magnetic field" menu, we added "Ampere's Law" with cyl1, cyl3, and cyl4 selected. To build the magnetic field modelling, we used relative permeability to represent the constitutive relation, which can be presented by

$$B = \mu_0 \mu_r H \tag{1}$$

where $B$ is the magnetic flux density, $\mu_0$ is the permeability of the vacuum, $\mu_r$ is the relative permeability of the materials, and $H$ is the magnetic field strength. Additionally, $\mu_0$ is set as $4\pi \times 10^{-7}\,\mathrm{H\,m^{-1}}$. We then added "Magnetic Insulation" and "Initial Values" with cyl1, cyl2, cyl3, and cyl4 selected. In the "Initial Values," the "Magnetic vector" potential was selected to 0. Finally, we added "Coil" to cyl2. In the "Coil" setting, we set the "Conductor model" to "Homogenized multi-turn", the "Coil type" to "Numeric", the "Coil current" to 2 A, the "Number of turns" to 400, and the "Coil wire cross-section area" to 0.35 mm. In the "Input," the subcategory of "Coil," a cross-section surface was selected to define the input current.

*Magnetic Field Simulation: Mesh & Study*: The whole MRE valve module was meshed by selecting the "Mesh" function. The sequence type was set to "Physics-controlled mesh." And the "Element size" was set to "Normal." The minimum element quality was around 0.17, and the average element quality was around 0.6. Since the main function of the simulation was to confirm the magnetic field density of four different MRE membranes, the average element quality did not need to be high. Therefore, the average element quality of 0.6 satisfied our requirements. In the "Study," we added 2 steps. Step 1 was "Coil geometry analysis," and Step 2 was "Stationary." Then we clicked "Compute" to calculate the simulation.

*Magnetic Field Simulation: Results*: A "Slice plot" with the "Magnetic Flux Density Norm" was used to obtain the simulated magnetic field presented in the paper. The "Slice plot" was selected to the surface on the long side of the flow pass. "Rainbow" was selected in the "Coloring and Style."

*Flowrate-Current Profile Characterization*: A compressor (BB50D, Bambi Air Compressor LTD, with integrated reservoir) with pneumatic filter (AL20-F02-A, SMC) and regulator (AR20-F02-1-B, SMC) was used to keep the input pressure constant throughout the process. A pressure sensor (ADP60, Panasonic) was placed at the inlet of the valve to monitor this pressure. The current through the MRE valve was driven by a continuous DC power supply box with current reading (GPS-3303, GW-INSTEK). The flowrate through the valve under different amounts of electric current was recorded by a digital flowrate sensor (HAF 20SLPM AIR, Honeywell).

*Threshold Pressure Characterization*: A compressor (BB50D, Bambi Air Compressor LTD, with integrated reservoir) with a pneumatic filter (AL20-F02-A, SMC) and regulator (AR20-F02-1-B, SMC) was used to incrementally increase the input pressure applied to the valve from 0 kPa. This supply pressure was continuously monitored by a pressure sensor (ADP60, Panasonic) throughout the entire process. To detect any leakage of the valve, the volume flowrate sensor (HAF 20SLPM AIR, Honeywell) was directly connected to the valve output. Once the flowrate sensor came out with a reading larger than $5\,\mathrm{mL\,min^{-1}}$, the valve was identified as "leaked" and the input pressure then was recorded as the threshold pressure. Three independent trials were performed to ensure repeatability.

*Temperature Response Characterization*: The temperature readings were obtained by a digital temperature sensor (DS18B20, SMD). A piece of electric tape was used to ensure firm contact between the sensor and the MRE membrane. The constant electric current through the coil was supplied by a DC power supply box with current reading (GPS-3303, GW-INSTEK). The flowrate through the valve was recorded by a digital flowrate sensor (HAF 20SLPM AIR, Honeywell).

*Preparation of Pneumatic Actuator*: The pneumatic actuator used in this work was a PneuNet bending actuator.[31] We used the same fabrication technique as the original work. The main body containing the inflatable chambers and the strain-limiting bottom layer was cast individually at first with silicone (Eco-flex 00-30, Smooth-on, USA). They were then bonded together with the same type of silicone. The strain-limiting material used was paper (80 gsm). After curing, the actuator was connected to the MRE valve via a needle (18 G, blunt head) and silicone pipes (OD 2 mm, ID 1 mm).

*Tuning of PID Controller*: For controlling the flowrate and pressure, a microcontroller (Teensy 4.1) was used to implement the closed-loop PID controller. The gains of the PID controllers were tuned empirically to achieve a fast response without significant overshoot or steady-state error. Firstly, only the P gain was introduced to increase the response speed. The I gain was then increased to reduce the steady-state error. Finally, the D gain was brought in for suppressing oscillations. The detailed setup and parameters of the PID controllers are presented in Supporting Information S3.

## Supporting Information

Supporting Information is available from the Wiley Online Library or from the author.

## Acknowledgements

This work was supported by the Engineering and Physical Sciences Research Council (EPSRC) Grant EP/V000748/1; S. Wang was supported by the CSC-PAG Oxford Scholarship for his DPhil study; P. Zhang was supported by JSPS KAKENHI Grant No.21J13536.

## Conflict of Interest

The authors declare no conflict of interest.

## Data Availability Statement

The data that support the findings of this study are available from the corresponding author upon reasonable request.

## Keywords

magnetorheological elastomers, pneumatic actuators, proportional valve, soft robotics

Received: July 28, 2022
Revised: September 1, 2022
Published online: October 17, 2022

[1] N. El-Atab, R. B. Mishra, F. Al-Modaf, L. Joharji, A. A. Alsharif, H. Alamoudi, M. Diaz, N. Qaiser, M. M. Hussain, *Adv. Intell. Syst.* **2020**, *2*, 2000128.
[2] J. Walker, T. Zidek, C. Harbel, S. Yoon, F. S. Strickland, S. Kumar, M. Shin, *Actuators*, Vol. *9*, Multidisciplinary Digital Publishing Institute, Basel, Switzerland **2020**, p. 3.
[3] B. Wijnen, E. J. Hunt, G. C. Anzalone, J. M. Pearce, *PloS One* **2014**, *9*, e107216.

[4] B. Zhang, J. Chen, X. Ma, Y. Wu, X. Zhang, H. Liao, *Soft Rob.* **2021**, unpublished.
[5] P. Rothemund, A. Ainla, L. Belding, D. J. Preston, S. Kurihara, Z. Suo, G. M. Whitesides, *Sci. Rob.* **2018**, *3*, eaar7986.
[6] S. Wang, L. He, P. Maiolino, *IEEE Rob. Autom. Lett.* **2021**, *7*, 112.
[7] J. D. Hubbard, R. Acevedo, K. M. Edwards, A. T. Alsharhan, Z. Wen, J. Landry, K. Wang, S. Schaffer, R. D. Sochol, *Sci. Adv.* **2021**, *7*, eabe5257.
[8] D. J. Preston, P. Rothemund, H. J. Jiang, M. P. Nemitz, J. Rawson, Z. Suo, G. M. Whitesides, *Proc. Natl. Acad. Sci.* **2019**, *116*, 7750.
[9] S. Wang, L. He, P. Maiolino, *IEEE Rob. Autom. Lett.* **2022**, *7*, 3412.
[10] M. P. Nemitz, C. K. Abrahamsson, L. Wille, A. A. Stokes, D. J. Preston, G. M. Whitesides, in *2020 3rd IEEE Int. Conf. Soft Robotics (RoboSoft)*, IEEE, Piscataway, NJ **2020**, pp. 7–12.
[11] R. Diteesawat, T. Helps, M. Taghavi, J. Rossiter, *Sci. Rob.* **2021**, *6*, eabc3721.
[12] S. Xu, Y. Chen, P. H. Nak-seung, K. P. Becker, R. J. Wood, *Proc. Natl. Acad. Sci.* **2021**, *118*, 34.
[13] P. Polygerinos, N. Correll, S. A. Morin, B. Mosadegh, C. D. Onal, K. Petersen, M. Cianchetti, M. T. Tolley, R. F. Shepherd, *Adv. Eng. Mater.* **2017**, *19*, 1700016.
[14] R. A. S. I. Subad, L. B. Cross, K. Park, *Appl. Mech.* **2021**, *2*, 356.
[15] T. George Thuruthel, Y. Ansari, E. Falotico, C. Laschi, *Soft Rob.* **2018**, *5*, 149.
[16] D. Drotman, S. Jadhav, D. Sharp, C. Chan, M. T. Tolley, *Sci. Rob.* **2021**, *6*, eaay2627.
[17] B. Eryilmaz, B. H. Wilson, *J. Franklin Inst.* **2006**, *343*, 48.
[18] K. J. McDonald, L. Kinnicutt, A. M. Moran, T. Ranzani, *IEEE Rob. Autom. Lett.* **2022**, *7*, 3914.
[19] M. S. Kalairaj, H. Banerjee, K. S. Kumar, K. G. Lopez, H. Ren, *Bioengineering* **2021**, *8*, 127.
[20] J. M. Ginder, M. E. Nichols, L. D. Elie, J. L. Tardiff, in *Smart Structures and Materials 1999: Smart Materials Technologies*, Vol. *3675*, SPIE, Newport Beach, California **1999**, pp. 131–138.
[21] A. G. Dez, C. R. Tubio, J. G. Etxebarria, S. Lanceros-Mendez, *Adv. Eng. Mater.* **2021**, *23*, 2100240.
[22] M. Zhu, M. Yu, S. Qi, J. Fu, *Smart Mater. Struct.* **2018**, *27*, 055017.
[23] S.-Y. Tang, X. Zhang, S. Sun, D. Yuan, Q. Zhao, S. Yan, L. Deng, G. Yun, J. Zhang, S. Zhang, W. Li, *Adv. Funct. Mater.* **2018**, *28*, 1705484.
[24] S. Kashima, F. Miyasaka, K. Hirata, *IEEE Trans. Magn.* **2012**, *48*, 1649.
[25] P. Zhang, M. Kamezaki, Z. He, H. Sakamoto, S. Sugano, *IEEE Rob. Autom. Lett.* **2021**, *6*, 8181.
[26] R. Guan, H. Zheng, Q. Liu, K. Ou, D.-S. Li, J. Fan, Q. Fu, Y. Sun, *Compos. Sci. Technol.* **2022**, *223*, 109409.
[27] V. Skfivan, O. Sodomka, F. Mach, in *2019 2nd IEEE Int. Conf. Soft Robotics (RoboSoft)*, IEEE, Piscataway, NJ **2019**, pp. 126–130.
[28] H. Wang, M. Totaro, A. A. Blandin, L. Beccai, in *2019 2nd IEEE Int. Conf. Soft Robotics (RoboSoft)*, IEEE, Piscataway, NJ **2019**, pp. 242–248.
[29] H. Böse, R. Rabindranath, J. Ehrlich, *J. Intell. Mater. Syst. Struct.* **2012**, *23*, 989.
[30] A. K. Bastola, M. Hossain, *Composites, Part B* **2020**, *200*, 108348.
[31] B. Mosadegh, P. Polygerinos, C. Keplinger, S. Wennstedt, R. F. Shepherd, U. Gupta, J. Shim, K. Bertoldi, C. J. Walsh, G. M. Whitesides, *Adv. Funct. Mater.* **2014**, *24*, 2163.
[32] A. K. Bastola, M. Paudel, L. Li, *J. Intell. Mater. Syst. Struct.* **2018**, *29*, 2946.